# Synthesis and Cathodoluminescence of Undoped and $Cr^{3+}$-Doped Sodium Titanate Nanotubes and Nanoribbons

**Carlos Díaz-Guerra,*,† Polona Umek,‡ Alexandre Gloter,§ and Javier Piqueras†**

*Departamento de Física de Materiales, Facultad de Ciencias Físicas, Universidad Complutense de Madrid, E-28040 Madrid, Spain, Jožef Stefan Institute, Jamova cesta 39, SI-1000 Ljubljana, Slovenia, and Laboratoire de Physique des Solides, Université Paris Sud, CNRS UMR8502, F-91405 Orsay, France*

*Received: January 19, 2010; Revised Manuscript Received: April 5, 2010*

We report on the synthesis of $Cr^{3+}$-doped sodium titanate nanotubes and nanoribbons by a hydrothermal method. The presence of dopant ions in these nanostructures was confirmed by high angle annular dark field scanning transmission electron microscopy in combination with electron energy loss spectroscopy measurements. Luminescence properties of undoped and $Cr^{3+}$-doped sodium titanate nanotubes and nanoribbons were investigated by cathodoluminescence in the scanning electron microscope. A broad visible band in the range 1.7−2.7 eV is observed in these nanostructures. Such emission is similar to that observed in bulk anatase $TiO_2$ and titanate powders, and is related to $TiO_6$ octahedra, which is a common feature to all the samples investigated. Near-infrared emission, sometimes attributed to $Ti^{3+}$ interstitials, is observed in bulk powders but is absent in the titanate nanotubes and nanoribbons. Incorporation of $Cr^{3+}$ between the titanate layers of the nanostructures is revealed by the characteristic intraionic emission line at 1.791 eV. Sodium titanate nanoribbons appear to be an effective host for optically active $Cr^{3+}$ ions, as compared with nanotubes or bulk powder.

## 1. Introduction

In recent years, an increasing activity relates to nanostructured materials because of the improved properties of structures with high surface to volume ratio. One of the materials of interest is titanium dioxide ($TiO_2$ or titania), which has been extensively investigated due to its applications[1] in gas sensing, photocatalysis, solar cells, and other fields. In particular, titania nanoparticles[2−5] as well as nanotubes and nanowires[6−11] have been synthesized by different methods. In addition to titania, titania-based materials—such as alkali titanates—are also studied in bulk and nanostructured form for potential applications in ion-exchange processes, photocatalysis, gas sensors, or fuel-cell electrolytes.[12−16] Precisely, titanate nanotubes with a large active area, as compared with other nanostructures, would be good candidates for catalysis applications. Hydrothermal synthesis of sodium titanate nanotubes (NaTiNTs),[15,16] which enables relatively large amounts of high-quality material to be grown, has generated great interest. Nanotubes synthesized in this way have been found to show high metal cation intercalation reactivity,[17] which suggests potential applications in ion-exchange and separation processes. Moreover, NaTiNTs are considered as promising materials for energy storage based on lithium intercalation.[18] Sodium titanate nanoribbons (NaTiNRs) have also been synthesized under hydrothermal conditions and exhibited catalytic ability for reduction of $NO_2$ gas, but high differences in adsorption and catalytic behavior were found between nanotubes and nanoribbons.[19,20] Titania-based nanotubes show intense photoluminescence in the visible range,[6] so that nanotubes and other nanostructures have potential optical applications. Contrary to the case of titania, there are only a few reports on the luminescence of NaTiNTs and other titanate nanostructures. In ref 21, the photoluminescence spectrum of NaTiNTs was found to consist of a band peaked at 390 nm (3.17 eV), while Riss et al.[22] observed an optical absorption edge at 3.2 eV and a photoluminescence peak at 2.4 eV in sodium titanate nanowires and nanotubes.

In this work, the luminescence of NaTiNTs and NaTiNRs and the effect of $Cr^{3+}$ doping on the emission have been investigated by cathodoluminescence (CL) in a scanning electron microscope (SEM). The luminescence of the nanostructures has been compared with that of bulk, pure, and $Cr^{3+}$-doped sodium titanate powder, and with $TiO_2$ anatase powder. Structural and compositional characterization of the nanotubes and nanoribbons has been carried out by X-ray diffraction (XRD), high-resolution transmission electron microscopy (HRTEM), SEM, energy dispersive X-ray spectroscopy (EDS), and high angle annular dark field scanning transmission electron microscopy (HAADF-STEM) in combination with electron energy loss spectroscopy (EELS).

## 2. Experimental Methods

The samples investigated were sodium titanate nanotubes (**NaTiNTs**) and nanoribbons (**NaTiNRs**) and both undoped and $Cr^{3+}$-doped (**Cr@NaTiNTs**, **Cr@NaTiNRs**). $TiO_2$ anatase powder, Cr-doped $TiO_2$ powder (**Cr@TiO$_2$**), as well as undoped and Cr-doped sodium hexatitanate powders (**NaTiP**, **Cr@NaTiP**) were used as reference samples.

**2.1. Synthesis. NaTiNTs** and **NaTiNRs** were synthesized from anatase $TiO_2$ (Aldrich, 325 mesh) and 10 M NaOH (Aldrich) at 135 and 175 °C. Detailed reaction conditions are described in ref 23.

**Cr@NaTiNTs** and **Cr@NaTiNRs** were synthesized in two stages. In the first stage, $TiO_2$ doped with 1.8 wt % of $Cr^{3+}$ (**Cr@TiO$_2$**) was prepared by the sol−gel method with tetrai-

* To whom correspondence should be addressed. E-mail: cdiazgue@fis.ucm.es.
† Universidad Complutense de Madrid.
‡ Jožef Stefan Institute.
§ Université Paris Sud.

10.1021/jp1005132 
Published on Web 04/20/2010

sopropyl titanate [$Ti(OCH(CH_3)_2$] (Aldrich) as a titanium source and chromium(III) nitrate nonahydrate [$Cr(NO_3)_3 \cdot 9H_2O$] (Fluka) as a source of $Cr^{3+}$.[24] In a typical reaction, 48 mL of $Ti(OCH(CH_3)_2$ was diluted in a mixture of 150 mL of *i*PrOH and 50 mL of EtOH. Then, a solution of 1.88 g of $Cr(NO_3)_3 \cdot 9H_2O$ dissolved in 14 mL of $H_2O$ and 60 mL of EtOH was slowly added. The reaction mixture was aged under constant stirring overnight. Starting sol was then slowly heated to remove *i*PrOH and EtOH. The obtained powder was dried for 12 h at 100 °C and finally annealed at 400 °C for 3 × 16 h. In the second stage, **Cr@NaTiNTs** and **Cr@NaTiNRs** were synthesized from 2 g of **Cr@$TiO_2$** and 25 mL of 10 M NaOH (Aldrich), using a procedure analogous to that described in ref 23. A Teflon-lined autoclave was filled to 23 mL (degree of filling 88%) and held during 72 h at 125 and 190 °C for nanotubes and nanoribbons synthesis, respectively. The resulting light green product was dispersed into 100 mL of deionized water and filtered. The material caught on the filter was subsequently washed with 50 mL of EtOH and dried overnight at 100 °C.

Sodium titanate (**NaTiP**) and $Cr^{3+}$-doped sodium titanate (**Cr@NaTiP**) powders were prepared by heating a mixture of $Na_2CO_3$ (Fluka) and $TiO_2$/ **Cr@$TiO_2$** in a molar ratio of 1:3 at 800 °C for 60 h. Details of the procedure are described in ref 25.

**2.2. Characterization Techniques.** The morphology of the synthesized materials was investigated with a Carl Zeiss Supra 35LV field emission scanning electron microscope (FE-SEM) and a Jeol JEM-2100 transmission electron microscope (TEM). The elemental composition of the samples was investigated by energy dispersive X-ray spectroscopy (EDS) in the FE-SEM. Samples for FE-SEM were prepared by depositing water suspensions on a conducting carbon tape fixed on aluminum sample holders. For TEM measurements, the samples were first dispersed in MeOH with the help of an ultrasonic bath. A drop of dispersion was then deposited on a carbon-coated Ni grid. STEM-HAADF and STEM-EELS measurements were performed with a dedicated scanning-transmission electron microscope (Vacuum Generators HB501) equipped with a home-modified Gatan spectrometer. Atomically resolved STEM-HAADF images have been acquired by using a $C_3/C_5$ spherical aberration-corrected microscope Nion U-STEM working at 100 keV. EELS were acquired with use of a modified GATAN EELS system with a back- illuminated charge-coupled device camera.

The powder X-ray diffraction (XRD) patterns were obtained on a Bruker AXS D4 Endeavor diffractometer, using Cu Kα radiation.

CL measurements were carried out in a Hitachi S-2500 SEM, using an accelerating voltage of 20 kV at temperatures between 80 and 295 K. CL spectra in the range 300−800 nm (4.14−1.55 eV) were recorded with a charge coupled device camera with a built-in spectrograph (Hamamatsu PMA-111) and corrected for system response. CL spectra in the near-infrared range 800−1800 nm (1.55−0.69 eV) were recorded with a Hamamatsu R5509-43 photomultiplier and a computer-controlled Oriel 74100 monochromator.

## 3. Results and Discussion

Doping of sodium titanate nanotubes and nanoribbons with $Cr^{3+}$ was achieved by an in situ doping method, meaning in the present case that the starting $TiO_2$ material used for the synthesis of **Cr@NaTiNRs** and **Cr@NaTiNTs** was already doped with $Cr^{3+}$ ions. As described in ref 24, this approach leads to a more homogeneous distribution of dopant ions in the titanate matrix.

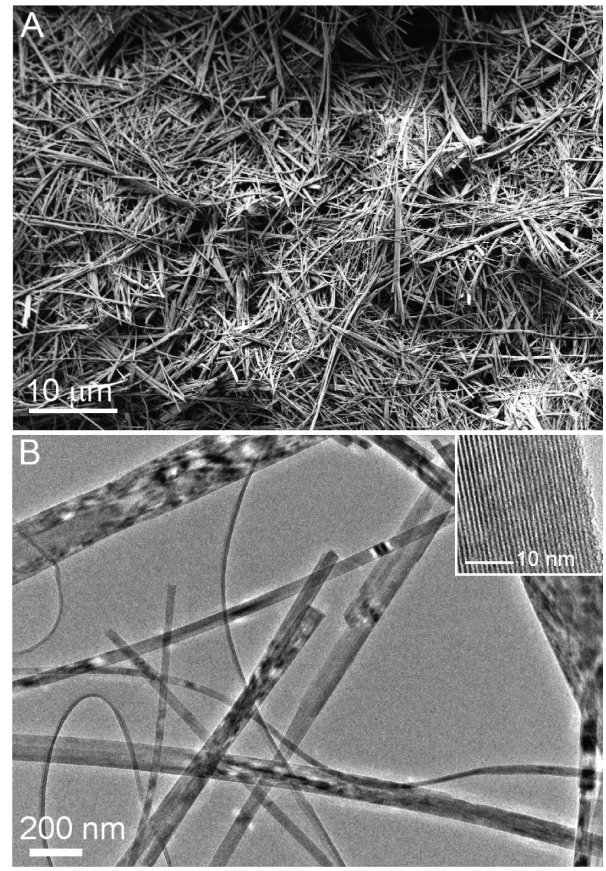


**Figure 1.** SEM (a) and TEM micrographs (b) of chromium-doped sodium titanate nanoribbons (**Cr@NaTiNRs**). The inset of part b shows the layered structure of the ribbon. The interlayer distance is around 0.71 nm.

**3.1. SEM and TEM Characterization.** The morphology of the synthesized materials was investigated by SEM and TEM. Microscopy images of **Cr@NaTiNRs** (Figure 1) and **Cr@NaTiNTs** (Figure 2) reveal that both materials were synthesized with high yields and uniform morphologies. In addition, no significant differences were found between the dimensions of the doped nanostructures and those characteristic of undoped sodium titanate nanoribbons and nanotubes.[23] Doped nanoribbons grow up to 10 $\mu$m in length while their diameters are in the range 30−300 nm. On the other hand, **Cr@NaTiNTs** are much shorter (up to 500 nm), with diameters between 8 and 12 nm (Figure 2). Besides nanotubes, some partly rolled slabs are also observed in the **Cr@NaTiNTs** sample (Figure 2c). This morphology was previously reported in the case of $Cu^{2+}$-doped titanate nanotubes,[24] where actually most of the sample consisted of partly rolled titanate slabs, not nanotubes. Just the opposite is observed for the **Cr@NaTiNTs** investigated here, where the nanotube morphology prevails. The different morphologies may be related to different positions occupied by the dopant atoms in the titanate structure. Since this particular information is difficult to extract from XRD data, further structural characterization with EXAFS (Extended X-ray Absorption Fine Structure) is in progress to gain insight on this issue. Actually, while intercalation of Cu atoms between the titanate slabs was reported for Cu@NTs,[24] preliminary EXAFS results suggest that Cr atoms probably substitute Ti atoms in the titanate lattice.

According to TEM micrographs, $Cr^{3+}$-doped $TiO_2$ (**Cr@$TiO_2$**) powder consists of fine nanoparticles (Figure 3a) with diameters around 10 nm, while chromium-doped sodium titanate powder

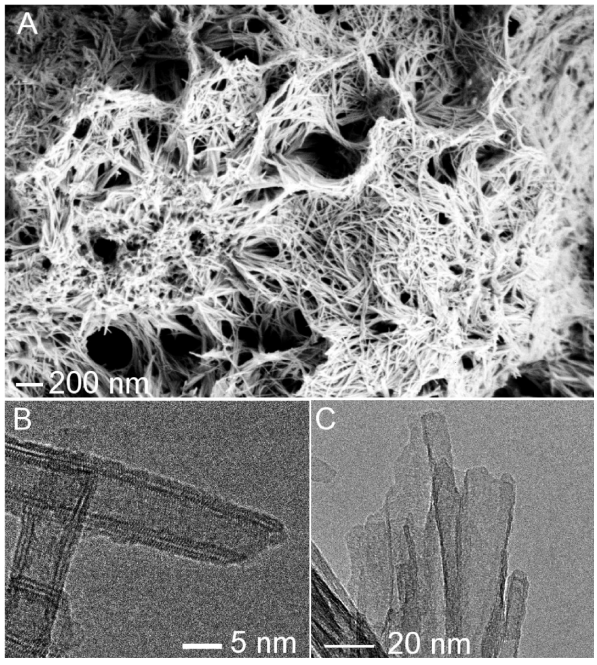


**Figure 2.** SEM (a) and TEM (b,c) micrographs of chromium-doped sodium titanate nanotubes (**Cr@NaTiNTs**). Besides nanotubes (b), partly rolled titanate slabs are also present in the sample (c).

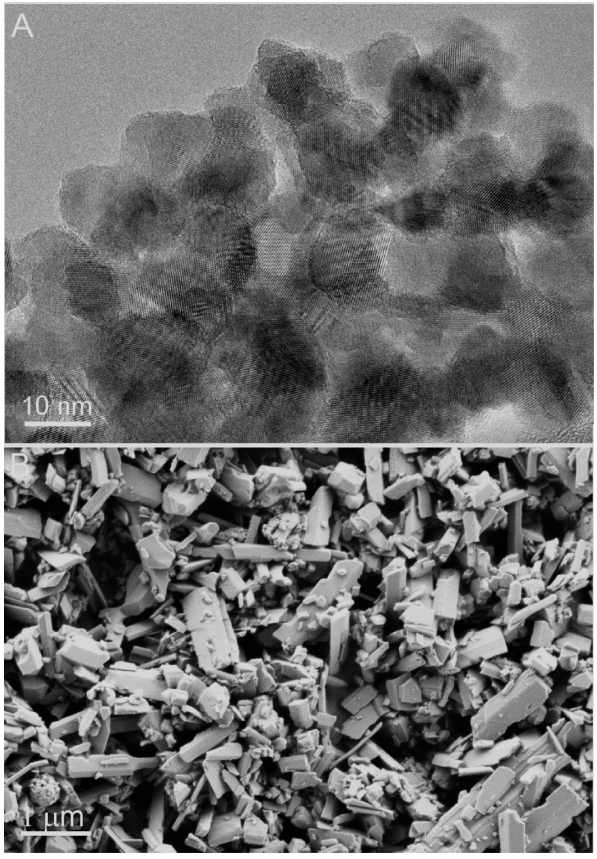


**Figure 3.** (a) TEM micrograph of chromium-doped $TiO_2$ (**Cr-$TiO_2$**), which consists of approximately 10−15 nm sized nanoparticles. (b) SEM image of **Cr@NaTiPs**.

(**Cr@NaTiPs**) consists of micrometer sized particles (Figure 3b). The morphology and particle size of undoped titanate powder (**NaTiP**) are similar to those of **Cr@NaTiPs**.

**3.2. Elemental Analysis.** To determine the chromium content in the prepared materials, EDS elemental analyses were performed. The results for **Cr@NaTiNRs**, **Cr@NaTiNTs**, **Cr@$TiO_2$**, **NaTiNRs**, **NaTiNTs**, **NaTiPs**, and **Cr@NaTiPs** are summarized in Table 1. Surprisingly, the chromium content for **Cr@NaTiNRs** and **Cr@NaTiNTs** differs notably, although both samples were prepared from **Cr@$TiO_2$** under the same conditions. Only the reaction temperature was different, 125 °C for **Cr@NaTiNTs** and 190 °C for **Cr@NaTiNRs**. The lower amount of chromium found in **Cr@NaTiNRs** can be explained first by the formation of soluble poly-hydroxyl chromium(III) species in the reaction mixture at higher temperatures[26,27]—which do not tend to incorporate between the titanate layers or do not adsorb on the surface of the nanostructures—and second by the interlayer distance between titanate layers. Such a distance is smaller for nanoribbons than for nanotubes[20] and, consequently, the Cr content is four times lower in **Cr@NaTiNRs** than in **Cr@NaTiNTs**.

**TABLE 1: Elemental Analysis for $Cr^{3+}$-Doped NaTiNRs (Cr@NaTiNRs) and NaTiNTs (Cr@NaTiNTs), Pristine NaTiNRs and NaTiNTs, $Cr^{3+}$-Doped $TiO_2$ (Cr-$TiO_2$), and $Cr^{3+}$-Doped (Cr@NaTiP) and Undoped Titanate Powders (NaTiP)**

| sample | Na, atom % | Ti, atom % | O, atom % | Cr, atom % |
|---|---|---|---|---|
| **Cr@NaTiNRs** | 12.1 | 21.0 | 66.8 | 0.1 |
| **Cr@NaTiNTs** | 9.7 | 24.0 | 65.9 | 0.4 |
| **Cr-$TiO_2$** | | 29.4 | 69.3 | 0.8 |
| **NaTiNRs** | 11.5 | 23.5 | 65.0 | |
| **NaTiNTs** | 13.0 | 22.1 | 64.7 | |
| **NaTiP** | 7.1 | 28.5 | 64.4 | |
| **Cr@NaTiP** | 7.0 | 27.5 | 65.2 | 0.3 |

**3.3. HAADF-STEM and EELS Study.** The presence of chromium in **Cr@NaTiNTs** and **Cr@NaTiNRs** was unambiguously proven by the elemental analysis performed by SEM-EDS (Table 1). HAADF-STEM/HRTEM in combination with EELS was used for assessment of the local Cr content and to determine if these two samples contained nanometer-sized particles with a higher dopant content. Panels a and b of Figure 4 respectively show a HAADF-STEM image of a chromium-doped sodium titanate nanotube and elemental line profiles across the same nanotube obtained by EELS. The O and Ti profiles show a complete correlation, whereas the Cr profile fluctuates due to the lower content of this element in the material. These observations confirm the incorporation of Cr to the titanate nanotubes, which seems to be mainly located on the surface of the nanostructure. Panels c and d of Figure 4 show representative HAADF-STEM images of **Cr@NaTiNRs**. The images reveal that no small nanoparticles are present in this sample and that the nanoribbons are crystalline. The measured interlayer distance (Figure 4d) is about 0.71 nm, which agrees well with that of the (101) planes for this type of material.[20,28]

Figure 4e shows another HAADF-STEM image of a Cr-doped nanotube and the corresponding EELS spectrum, revealing the incorporation of Cr to the nanostructure. EELS spectra were collected either on areas with lateral sizes of tens of nanometers, typically comprising about a dozen of nanotubes/nanoribbons, or on individual nanostructures, as shown in Figure 4e. After quantification, the following average elemental concentrations were obtained: 38.4% of Ti, 60.3% of O, and 1.3% of Cr for **Cr@NaTiNT**s and 28.6% of Ti, 70.5% of O, and 1.0% of Cr for **Cr@NaTiNRs**. Because of the low EELS accuracy, due to the difficult edge extraction for Cr and the weak phase stability under the TEM electron beam, these results just confirm that Cr is present at the percent level on a nanometer scale. The amount of Na was not quantified since the Na 1s excitation is

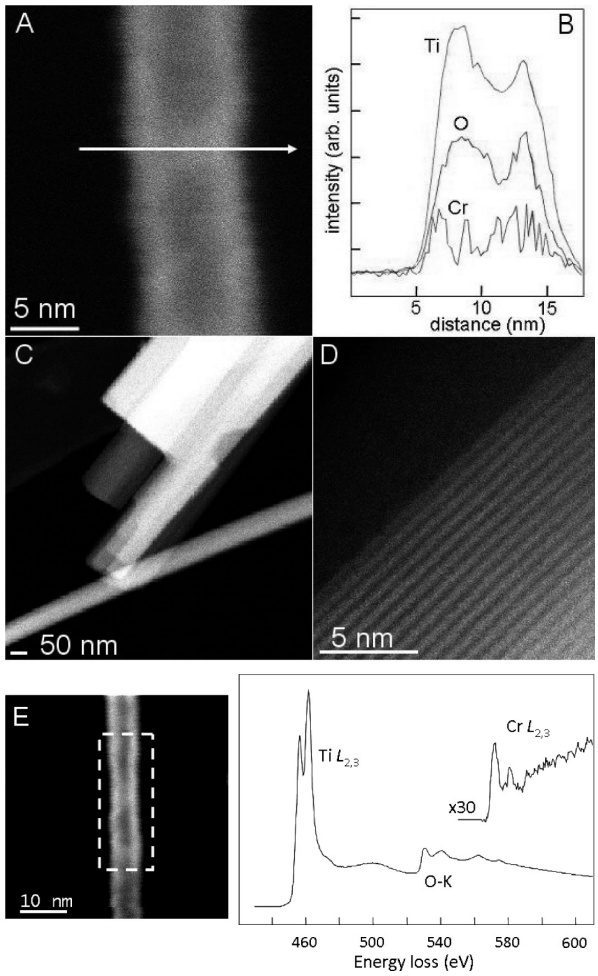


**Figure 4.** (a) HAADF-STEM image of a chromium-doped titanate nanotube (**Cr@NaTiNT**). (b) Ti, O, and Cr intensities of the EELS signal for the line profile across the nanotube shown in part a. Ti 2p and O 1s excitations have been integrated over 40 eV while the Cr 2p excitation has been integrated over 18 eV. With respect to the Ti signal, O and Cr signals have been respectively multiplied by a factor of 3 and 40. (c, d) HAADF-STEM images of $Cr^{3+}$-doped sodium titanate nanoribbons (**Cr@TiNRs**). The interlayer distance between fringes in part d is 0.71 nm. (e) HAADF-STEM micrograph of another **Cr@NaTiNT** and EELS spectrum from the area marked in the image.

located at 1072 eV, too high in energy to be efficiently collected simultaneously to the Ti and O edges.

**3.4. XRD Measurements.** To study the structures of the doped nanoribbon and nanotube samples and to compare them with those of pristine **NaTiNRs** and **NaTiNTs**, XRD measurements were carried out (Figure 5). XRD patterns of **Cr@NaTiNRs** and **Cr@NaTiNTs** are similar to those of pristine **NaTiNRs** and **NaTiNTs**.[23,24] The XRD pattern of chromium-doped titania shows a mixture of anatase and rutile phases, while the XRD pattern of chromium-doped titanate powder corresponds to the $Na_2Ti_6O_{13}$ structure (JCPDS 73-1398). Additional peaks (marked with asterisks) that correspond to the rutile phase are observed in the XRD profiles of **Cr@NaTiP**. The XRD pattern of **NaTiP** (not shown) is similar to that of **Cr@NaTiP**.

**3.5. Cathodoluminescence Study.** The luminescence properties of the different samples were investigated by cathodoluminescence (CL) in the SEM. CL spectra of the reference anatase powder show intense emission in the visible range in the studied temperature range, from 80 to 300 K. The spectra consist of a complex broad band extending from about 1.7 to

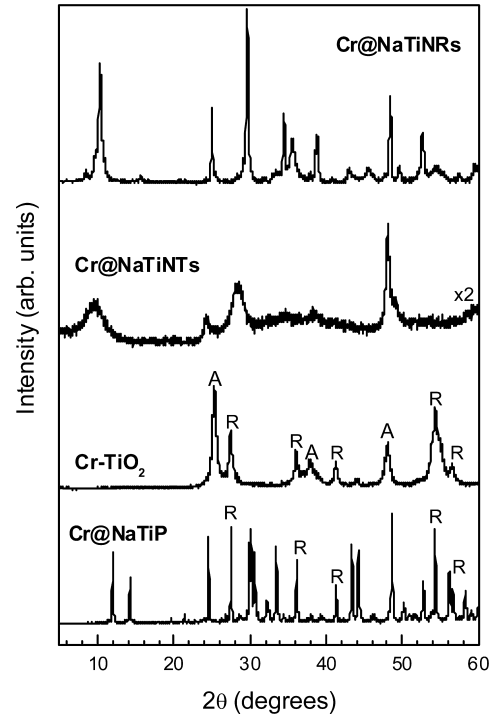


**Figure 5.** XRD patterns of chromium-doped sodium titanate powder (**Cr@NaTiP**), chromium-doped $TiO_2$ (**Cr-$TiO_2$**), chromium-doped titanate nanotubes (**Cr@NaTiNTs**), and nanoribbons (**Cr@TiNRs**). The letters A and R stand for anatase and rutile phase, respectively.

2.7 eV. By varying temperature or excitation conditions in SEM, mainly beam current density, the relative weight of the different components of the broad band changes. This is apparent in the CL spectra shown in Figure 6a, with the band peaked at about 2.36 eV at 80 K and at about 2.56 eV at 290 K. Gaussian deconvolution (Figure 6b) reveals that four components, centered at about 2.71, 2.56, 2.36, and 2.03 eV, contribute to the observed emission. The anatase powder also shows CL emission in the near-infrared range, with a broad band peaked at about 1.35 eV. Figure 7 shows the Gaussian deconvolution of this broad band, with components at 1.52, 1.45, 1.35, and 1.24 eV. The intensity of the infrared emission decreases by increasing temperature and is quenched at about 240 K, as measured with our detection system.

CL spectra of undoped sodium titanate powder (**NaTiP**) show a broad band peaked at about 2.56 eV. The 2.36 eV band, dominant in the anatase powder, is also observed in these spectra (Figure 8a, solid line). It appears that anatase and undoped titanate powders have similar complex luminescence bands in the visible range, but with different weight of their components. No infrared emission was detected in the undoped titanate powder. **Cr@NaTiP** presents lower luminescence intensity than undoped powder, but their spectra have similar shapes in the visible range, with the exception of a weak band at 1.90 eV not observed in undoped powder. Characteristic emission of $Cr^{3+}$ ions was not observed (Figure 8a, dashed line). This doped powder also shows infrared emission with at least two peaks, also detected in anatase powder, centered at 1.43 and 1.37 eV, respectively (Figure 8b).

Sodium titanate nanotubes show CL emission in the visible range but no emission in the infrared range was detected. Figure 9a shows the CL spectrum of **NaTiNTs** measured at different temperatures. The main band, peaked at any temperature at about 2.48 eV, can be decomposed (not shown), with small deviations in the peak values, into the same four components as the visible

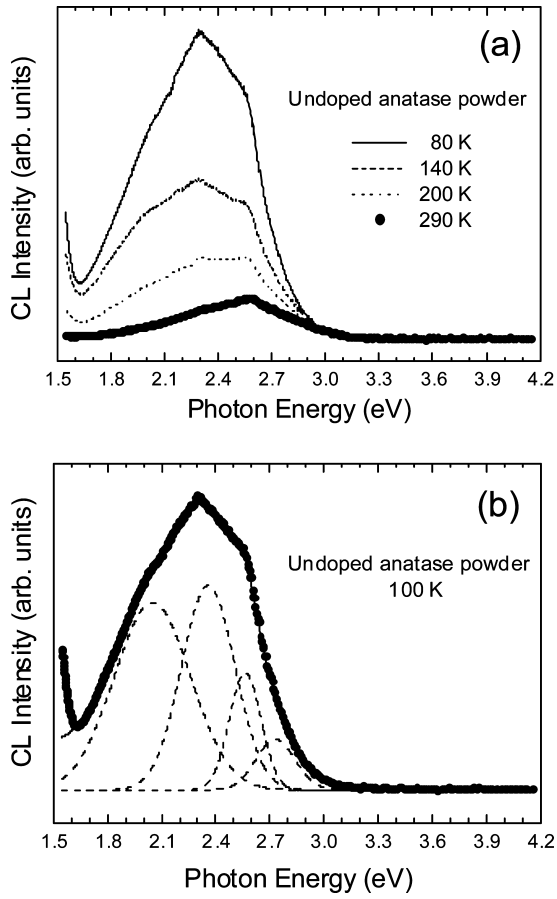


**Figure 6.** (a) CL spectra of undoped $TiO_2$ anatase powder recorded at several temperatures. (b) Gaussian deconvolution of a low-temperature (100 K) CL spectrum. Emission bands are found centered at 2.71, 2.56, 2.36, and 2.03 eV. Circles represent the experimental data while the solid line corresponds to the best-fit curve.

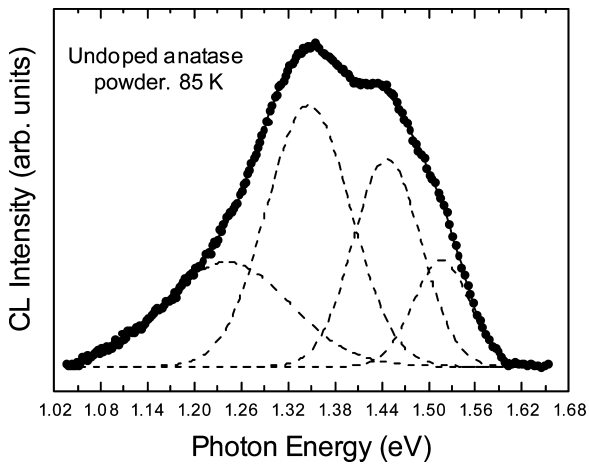


**Figure 7.** Gaussian deconvolution of an infrared CL spectrum recorded at 90 K from the undoped $TiO_2$ powder. Emission bands are found centered at 1.52, 1.45, 1.35, and 1.24 eV. The solid line corresponds to the best-fit curve while circles represent experimental data.

emission of the anatase powder. In addition, the nanotubes present a band at 3.33 eV, not observed in anatase. $Cr^{3+}$ doping of the sodium titanate nanotubes causes a strong reduction of the CL intensity. Actually, the emission at 80 K of the **Cr@NaTiNTs** is 5 to 10 times weaker than that of undoped material, so that it can be hardly detected at room temperature. Representative spectra of these doped nanotubes at 80 K are shown in Figure 9b. The spectra show peaks at about 2.57 and

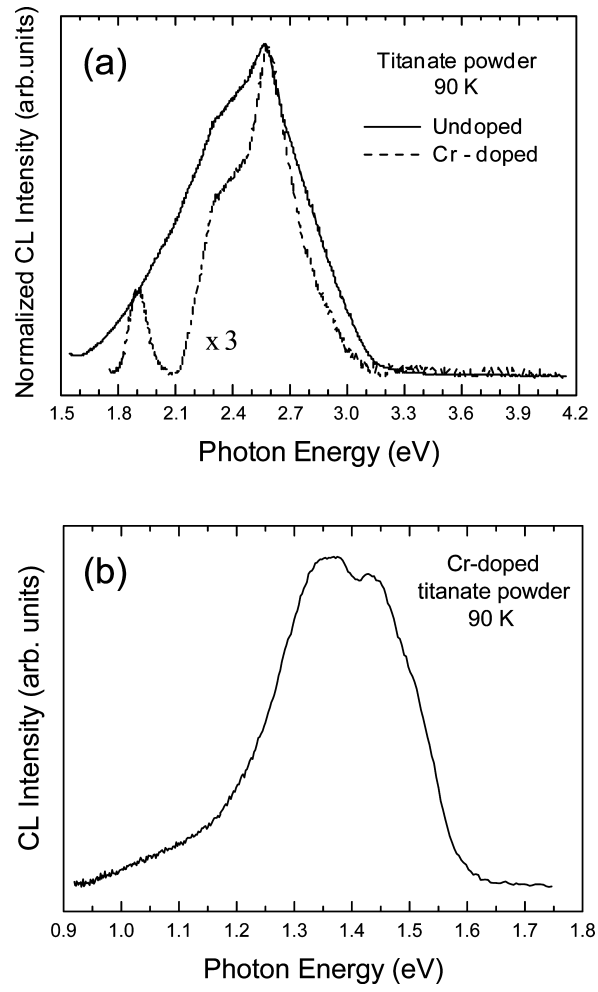


**Figure 8.** (a) Low-temperature (90 K) CL spectra of undoped (**NaTiP**) (solid line) and chromium-doped (dashed line) titanate powder (**Cr@NaTiP**). (b) Infrared CL spectrum recorded at 90 K from the chromium-doped titanate powder (**Cr@NaTiP**).

2.32 eV, close to the main peaks of anatase and of undoped nanotubes, as well as a broad emission with maximum at 3.3 eV. Luminescence of dopant chromium ions is apparent only in a fraction (20%) of the recorded spectra, dashed line in Figure 9b, by a sharp emission line at 1.791 eV (692.4 nm). This emission corresponds to the R-line of $Cr^{3+}$ ions in octahedral coordination, associated to $^2E \rightarrow {}^4A_2$ intraionic transitions.

Sodium titanate nanoribbons (**NaTiNRs**) show, as the nanotubes, luminescence in the visible range but not in the near-infrared range. The CL spectrum of the nanoribbons is shown in Figure 10a. Deconvolution of the observed band reveals the presence of four components, not shown in the figure, at similar energies to that observed in anatase and the nanotubes. Contrary to the case of **Cr@NaTiP** and **Cr@NaTiNTs**, the incorporation of $Cr^{3+}$ ions is readily detected in the CL spectra of $Cr^{3+}$-doped sodium titanate nanoribbons (Figure 10b). All spectra of nanoribbons, at any temperature in the investigated range of 85−300 K, show an intense $Cr^{3+}$ emission at 1.791 eV in addition to the broad band also observed in the undoped samples. In some CL spectra recorded on specific bunches of nanoribbons, the broad band is even quenched and only the $Cr^{3+}$ emission line is observed.

These results strongly suggest that defects or mechanisms similar to those responsible for the luminescence of $TiO_2$ may be involved in the luminescence emission of titanate nanostructures. The defect structure of $TiO_2$ includes $Ti^{3+}$ and $Ti^{4+}$

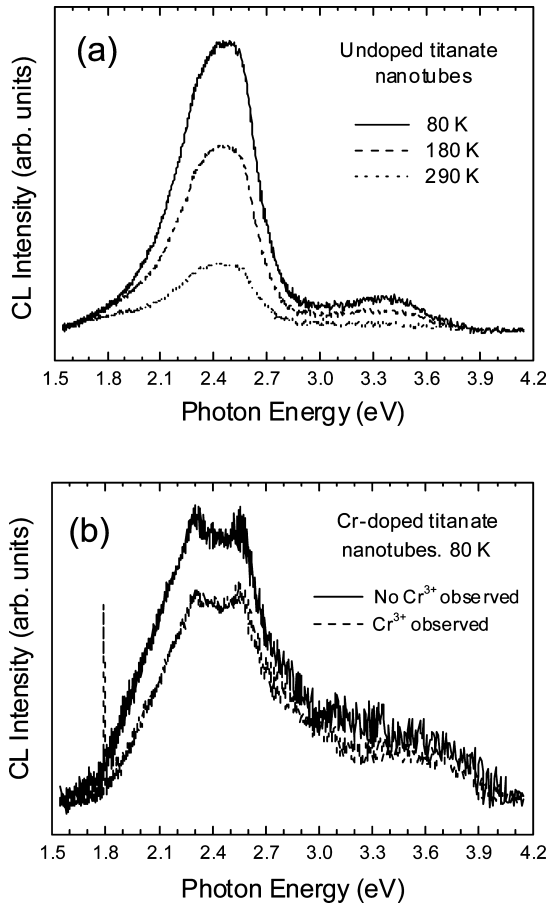


**Figure 9.** (a) Spectral distribution of the CL emission from undoped titanate nanotubes (**NaTiNTs**) measured at different temperatures. (b) CL spectra (90 K) of chromium-doped sodium titanate nanotubes (**Cr@NaTiNTs**).

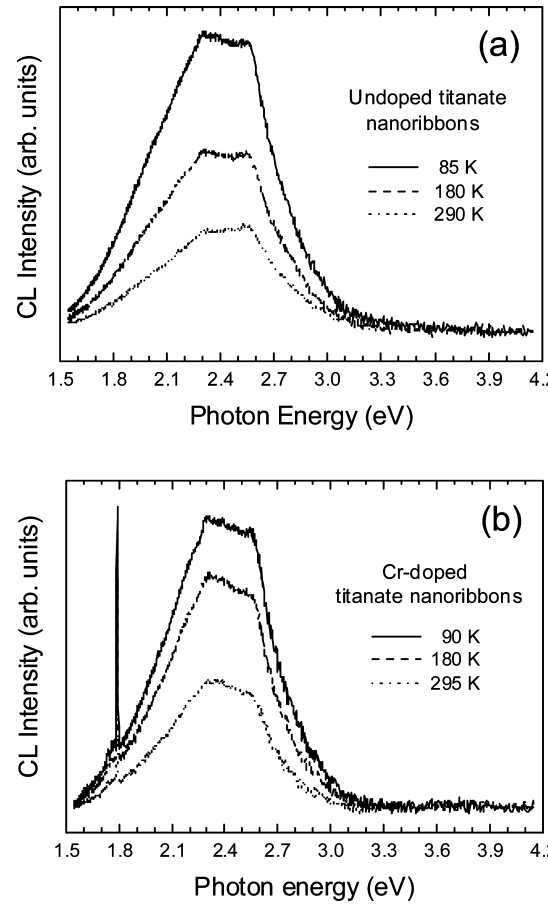


**Figure 10.** CL spectra of (a) undoped (**NaTiNRs**) and (b) $Cr^{3+}$-doped sodium titanate nanoribbons (**Cr@NaTiNRs**) measured at several temperatures.

interstitials, self-trapped excitons (STE), and oxygen-related defects. In $TiO_2$, each $Ti^{4+}$ ion is surrounded by an octahedron of six $O^{2-}$ ions. Defects can be formed by losing a neutral oxygen atom that causes two occupied O 2p levels in the valence band to be no longer available. The two electrons previously occupying those states migrate into the conduction band, the bottom of which is formed by Ti 3d states. Two neighboring Ti atoms receive an electron and defect states associated to the $Ti^{3+}$ are formed at about 0.7−0.8 eV below $E_F$.[29] Infrared emission at about 1.52 eV in rutile single crystals has been associated with $Ti^{3+}$ ions[30] and a similar band was observed in polycrystalline rutile and anatase.[31] This also would be the origin of the infrared band at about 1.52 eV observed in our anatase reference powder.

The existence of defect levels associated to oxygen vacancies has been reported, e.g.,[29−32] with shallow traps at energies in the range 0.27−0.87 eV below the conduction band. Other authors explain the photoluminescence emission in the visible range observed in anatase in terms of STE localized on $TiO_6$ octahedra,[33] since exciton trapping in anatase is enhanced due to lower octahedra coordination and longer bond lengths as compared with the rutile structure. The main visible luminescence band at about 2.4 eV, previously observed in $TiO_2$ and some titanate,s has been related to transitions associated with the $TiO_6$ octahedra. In particular, the 2.4 eV band reported in layered titanate nanostructures has been ascribed to deactivation of excitons trapped in the $TiO_6$ units.[22] We suggest that this is the origin of the main components of the visible band observed in all samples studied here, which have $TiO_6$ octahedra as a common structural unit.

The emission band at about 3.3−3.4 eV observed in some of the samples, titanate nanotubes or $Cr^{3+}$-doped $TiO_2$, may correspond to near band edge radiative transitions. Its presence and its intensity would depend in each sample on the probability of other recombination paths. The band gap energy for $TiO_2$ anatase is about 3.3 eV and the band gap values of 3.3 or 3.4 eV have been reported[34,35] for titanate nanotubes.

The CL results show clear differences in the incorporation of $Cr^{3+}$ active ions into the titanate powder and into the nanostructures. In the titanate powder, no CL emission from $Cr^{3+}$ ions has been detected, while CL spectra of both doped nanostructures, nanotubes and nanoribbons, show the characteristic emission line at 1.791 eV of $Cr^{3+}$. **Cr@NaTiNRs** appear to be especially favorable hosts for optically active $Cr^{3+}$ ions, whose emission line is observed in all recorded spectra, while in **Cr@NaTiNTs** this line appears only in a fraction of the corresponding CL spectra. The Cr content measured in the nanoribbons is lower than that measured in the nanotubes. This seems to favor the $Cr^{3+}$ emission, which may be due to a concentration quenching effect related to ion−ion interaction. Such a phenomenon has been previously reported in several Cr-doped oxides.[36] In that case, CL quenching may be due to energy migration through the excited level of the emitting ion to the same neighbor ions, forming pairs or clusters too small to be clearly detected by STEM-based techniques.

## 4. Conclusions

$Cr^{3+}$-doped sodium titanate nanotubes and nanoribbons have been grown under hydrothermal conditions from $Cr^{3+}$-doped

$TiO_2$ and NaOH (aq). The incorporation of dopant ions to the nanostructures has been assessed by HAADF-STEM microscopy combined with EELS spectroscopy as well as by EDS microanalysis. Luminescence properties of undoped and Cr-doped sodium titanate nanotubes and nanoribbons have been investigated and compared with the luminescence of reference anatase and titanate powders. A broad visible luminescence band, with main components at about 2.56 and 2.36 eV, suggested to be related to electronic transitions in $TiO_6$ octahedra, has been found in all the investigated samples. A broad near-infrared band in the range 1.2−1.5 eV, present in anatase and in some titanate powders, is not observed in the titanate nanostructures. This band is possibly associated with $Ti^{3+}$ interstitials. Cr doping induces partial quenching of the visible luminescence. Characteristic emission of $Cr^{3+}$ has been observed in the doped nanotubes and nanoribbons but not in doped powder. Nanoribbons appear to be favorable hosts for optically active $Cr^{3+}$ ions.

**Acknowledgment.** This work has been supported by MEC trough projects MAT2006-01259 and MAT2009-07882 and by the Slovenian Research Agency (J2-9217). P.U. and A.G. also acknowledge financial support from the European Union as a part of a Framework 6 program under a contract for an Integrated Infrastructure Initiative (reference 026019 ESTEEM).

## References and Notes

(1) Diebold, U. *Surf. Sci. Rep.* **2003**, *48*, 53.
(2) Madhusudan Reddy, K.; Manorama, S. V.; Ramachandra Reddy, A. *Mater. Chem. Phys.* **2002**, *78*, 239.
(3) Wu, Z. Y.; Zhang, J.; Ibrahim, K.; Xian, D. C.; Li, G.; Tao, Y.; Hu, T. D.; Bellucci, S.; Marcelli, A.; Zhang, O. H.; Gao, L.; Chen, Z. Z. *Appl. Phys. Lett.* **2002**, *80*, 2973.
(4) Tang, J.; Redl, F.; Zhu, Y.; Siegrist, T.; Brus, L. E.; Steigerwald, M. L. *Nano Lett.* **2005**, *5*, 543.
(5) Song, L.; Lam, Y. M.; Boothroyd, C.; Teo, P. W. *Nanotechnology* **2007**, *18*, 135605.
(6) Lei, Y.; Zhang, L. D.; Meng, G. W.; Li, G. H.; Zhang, X. Y.; Liang, C. H.; Chen, W.; Wang, S. X. *Appl. Phys. Lett.* **2001**, *78*, 1125.
(7) Du, G. H.; Chen, Q.; Che, R. C.; Yuan, Z. Y.; Peng, L. M. *Appl. Phys. Lett.* **2001**, *79*, 3702.
(8) Yao, B. D.; Chan, Y. F.; Zhang, X. Y.; Zhang, W. F.; Yang, Z. Y.; Wang, N. *Appl. Phys. Lett.* **2003**, *82*, 281.
(9) Pradham, S. K.; Reucroft, P. J.; Yang, F.; Dozier, A. *J. Cryst. Growth* **2003**, *256*, 83.
(10) Maestre, D.; Cremades, A.; Piqueras, J. *Nanotechnology* **2006**, *17*, 1584.
(11) Maestre, D.; Cremades, A.; Gregoratti, L.; Piqueras, J. *J. Nanosci. Nanotechnol.* **2008**, *8*, 6533.
(12) Hagfeldt, A.; Grätzel, M. *Chem. Rev.* **1995**, *95*, 49.
(13) Ramírez-Salgado, J.; Djurado, E.; Fabry, P. *J. Eur. Ceram. Soc.* **2004**, *24*, 2477.
(14) Anderson, M. W.; Klinowski, J. *Inorg. Chem.* **1990**, *29*, 3260.
(15) Kasuga, T.; Hiramatsu, M.; Hoson, A.; Sekino, T.; Niihara, K. *Langmuir* **1998**, *14*, 3160.
(16) Kasuga, T.; Hiramatsu, M.; Hoson, A.; Sekino, T.; Niihara, K. *Adv. Mater.* **1999**, *11*, 1307.
(17) Ma, R.; Sasaki, T.; Bando, Y. *Chem. Commun.* **2005**, 948.
(18) Li, J.; Tang, Z.; Zhang, Z. *Chem. Mater.* **2007**, *17*, 5848.
(19) Tsai, C.-C.; Teng, H. *Chem. Mater.* **2004**, *16*, 4352.
(20) Umek, P.; Cevc, P.; Jesih, A.; Gloter, A.; Ewels, C. P.; Arèon, D. *Chem. Mater.* **2005**, *17*, 5945.
(21) Sun, X.; Li, Y. *Chem.—Eur. J.* **2003**, *9*, 2229.
(22) Riss, A.; Berger, T.; Grothe, H.; Bernardi, J.; Diwald, O.; Knözinger, E. *Nano Lett.* **2007**, *7*, 433.
(23) Umek, P.; Korošec, R. C.; Janear, B.; Dominko, R.; Arèon, D. *J. Nanosci. Nanotechnol.* **2007**, *7*, 3502.
(24) Umek, P.; Pregelj, M.; Gloter, A.; Cevc, P.; Jaglièiæ, Z.; Èeh, M.; Pirnat, U.; Arèon, D. *J. Phys. Chem. C* **2008**, *112*, 15311.
(25) Yang, J.; Li, D.; Wang, X.; Yang, X.; Lu, L. *J. Mater. Sci.* **2003**, *38*, 2907.
(26) Rai, D.; Sass, B. M.; Moore, D. A. *Inorg. Chem.* **1987**, *26*, 345.
(27) Laswick, J. A.; Plane, R. A. *J. Am. Chem. Soc.* **1959**, *81*, 3564.
(28) Papa, A.-L.; Millot, N.; Saviot, L.; Chassagnon, R.; Heintz, O. *J. Phys. Chem. C* **2009**, *113*, 12682.
(29) Sanjines, R.; Tang, H.; Berger, H.; Gozzo, F.; Margaritondo, G.; Levy, F. *J. Appl. Phys.* **1994**, *75*, 2945.
(30) Fernández, I.; Cremades, A.; Piqueras, J. *Semicond. Sci. Technol.* **2005**, *20*, 239.
(31) Plugaru, R.; Cremades, A.; Piqueras, J. *J. Phys.: Condens. Matter* **2004**, *16*, S261.
(32) Rothschild, A.; Levakov, A.; Shapira, Y.; Ashkenasy, N.; Komem, Y. *Surf. Sci.* **2003**, *532−535*, 456.
(33) Montoncello, F.; Carotta, M. C.; Cavicchi, B.; Ferroni, M.; Giberti, A.; Guidi, V.; Malagú, C.; Martinelli, G.; Meinardi, F. *J. Appl. Phys.* **2003**, *94*, 1501.
(34) Gao, T.; Wu, Q.; Fjellvag, H.; Norby, P. *J. Phys. Chem. C* **2008**, *112*, 8548.
(35) Suetake, J.; Nosaka, A. Y.; Hodouchi, K.; Matsubara, H.; Nosaka, Y. *J. Phys, Chem. C* **2008**, *112*, 18474.
(36) Boulon, G. Transition Metal Ion Lasers—$Cr^{3+}$. In *Handbook of Laser Technology and Applications*; Webb, C., Jones, J., Eds.; IOP Publishing Ltd.: Bristol, UK, 2004; Vol. II, pp 307−338.

JP1005132